Ballistic structure in the electron distribution function of small semiconducting structures: General features and specific trends

Harold U. Baranger* and John W. Wilkins
Laboratory of Atomic and Solid State Physics, Cornell University, Ithaca, New York 14853-2501
(Received 23 September 1986)

In the hot-electron, ballistic transport regime, we have calculated the distribution function $f(v,x)$ for electrons in a submicron N^+-N^--N^+ GaAs structure by directly solving the coupled Poisson and Boltzmann equations using simple relaxation-time models. Ballistic electrons cause both the dominant peak in $f(v,x)$ throughout much of the N^- region and additional structure, ballistic echoes, because of intervalley transfer. Both phenomena can be traced to simple features of the potential energy curve which should occur in many device geometries. The structure in the distribution function responds to changes in the parameters—mobility, voltage, and lattice temperature—in the way expected for ballistic electrons: a larger mobility, a larger voltage, or a lower temperature makes the structure more prominent. By integrating over the distribution function, we calculate as a function of distance the current and the width of the distribution, expressed as an effective "temperature." The I-V characteristics are nearly linear for all the cases studied (as well as for the experiment) showing that the current is not a sensitive probe of ballistic structure. In fact, the current as a function of mobility saturates in the ballistic regime (high mobility) where the injection over the initial barrier determines the current. The distribution functions we calculate are far from being drifted Maxwellian in form so a thermodynamic temperature cannot be defined. However, in the near-equilibrium regime we show that "heating" and "cooling" are first order in the applied voltage in contrast to bulk behavior where heating is second order in the field. At higher voltages, the width of the distribution function varies dramatically from less than the equilibrium width at injection to much larger than the equilibrium width.

I. INTRODUCTION

The transport properties of small solid-state structures, those having a submicron dimension, have recently received increasing attention because of the surprising new phenomena in both semiconducting and metallic systems. For example, experiments have revealed transport via localized states in narrow inversion layers,[1] noise caused by single traps,[2] current modulation caused by optical-phonon emission,[3] and carrier cooling rates which are substantially different from the bulk values.[4] An especially intriguing transport mode, ballistic transport,[5] involves carriers traversing a submicron region without scattering. Detailed theoretical predictions[6–8] for the distribution of electrons in the ballistic regime, including a suggestion for the most practical way to see the effect,[6] have recently been confirmed directly by experiments,[9–12] though not under optimal ballistic conditions.

Transport in submicron semiconducting structures differs from transport in bulk material in three important ways: (i) the ease with which far-from-equilibrium situations are created because of the large electric fields in small structures, (ii) the importance of ballistic electrons once dimensions are of the same order as the mean free path, and (iii) the new effects introduced by the close proximity of boundaries where the electron density is usually varying rapidly. Thus, any calculation of transport in submicron semiconducting structures must include hot electrons, ballistic electrons, and spatial gradient effects. Here we present a calculation of transport in a simple semiconducting structure, concentrating on ballistic effects in a regime where hot electrons and spatial gradients are important. We extend the theoretical understanding of ballistic electrons with the first solution of the Boltzmann equation in a submicron structure in which the conduction band has the two valleys necessary to describe the semiconducting materials used experimentally, in particular GaAs.

The majority of previous work[13] on transport in submicron semiconducting structures used the drift-diffusion equation[14] in which the current is a sum of a drift term which employs a field-dependent mobility and a diffusion term with a field-dependent diffusivity. While this approach is simple and hence practical for complex device geometries, the physical basis of a field-dependent mobility and diffusion constant is questionable.[15] An alternative to the drift-diffusion equation is Monte Carlo simulation[16] in which one generates typical histories of many electrons and then averages over the ensemble to find the quantities of interest. While ideally very accurate, this approach suffers from uncertainty in the large number of input parameters and the considerable computation time needed to acquire enough statistics. A possible way to bridge the gap between the drift-diffusion approach and Monte Carlo simulation is to generate a hydrodynamiclike theory using velocity moments of the Boltzmann equation.[17–19] It is necessary in this approach to truncate the hierarchy of moment equations by making an assumption for the form of the distribution function. Often the distribution is assumed to be a drifted Maxwellian distribution;[17,19] we will see below that this assumption is questionable in lightly doped submicron structures in part because of the pres-

ence of ballistic electrons.

Here we fill in some of the middle ground between the drift-diffusion equation and Monte Carlo simulation by using a direct, numerical solution of the Boltzmann equation within the relaxation-time approximation. The use of the Boltzmann equation in our situation is perhaps problematical because of the large, rapidly varying electric field and the ballistic electrons. The Boltzmann equation has been rigorously justified on the basis of quantum transport theory only for slowly varying potentials;[20] however, it is not clear on what length scale the potential must be slowly varying. Some work suggests that the appropriate length scale is the thermal wavelength $[=(\hbar^2/2m^*kT)^{1/2}\approx 0.005\ \mu\text{m}]$,[20] which is certainly a lower bound on the length scale at which the Boltzmann equation breaks down, in which case our use of the Boltzmann equation is appropriate. Since no evaluation of the corrections to the Boltzmann equation in the spatially varying case has been made, it is difficult to determine the spatial scale at which the Boltzmann equation breaks down, and we therefore use the Boltzmann equation until future workers clarify this point. We note in support, however, that the Boltzmann equation works well in at least one other situation where the electric field varies rapidly on a length scale less than the mean free path, namely in explaining the anomalous skin effect.[21]

Within the Boltzmann-equation approach we make the relaxation-time approximation that all the scattering processes can be characterized by one or two scattering rates (per valley). As this approximation is not strictly valid for GaAs,[22] our goal here is to present a completely solved model calculation rather than a microscopic calculation as in the Monte Carlo approach discussed above. Our use of relaxation-time models, in addition to making the problem tractable, makes the structure caused by spatial inhomogeneities (such as ballistic electrons) obvious and more easily studied. In addition, one can easily vary the parameters in our models to look for trends, something users of the more sophisticated Monte Carlo simulation have not done. We consider two particular relaxation-time models in this work: one in which there is a single valley with $1/\tau$ independent of velocity, and a second in which there are two valleys with one of the four $1/\tau$ depending on the velocity parallel to the field while the other three rates are constant. The use of rates which are independent of velocity is consistent with our emphasis on the effects of spatial inhomogeneities rather than the details of the scattering processes. The fact that the rates depend at most on the velocity parallel to the field (rather than on the energy, for instance), implies that the distribution of velocities perpendicular to the field is Maxwellian; thus, all the nonequilibrium effects occur in the distribution parallel to the field and in this sense our treatment is one dimensional in velocity. Because our two-valley model reproduces the experimental velocity-field curve over a substantial field range,[23] this model contains at least as much information about the scattering processes as the drift-diffusion or hydrodynamic theories discussed above.

Our approach complements recent analytic work using the Boltzmann equation including a solution for optic-phonon scattering in a non-self-consistent potential,[24] and a solution for small spatial and time perturbations from a large-uniform-field situation.[25] Some of our results have been presented previously.[7,26] Here we first describe the universal aspects of both the structure we study and our previous results (Sec. II), then we describe the model used in the calculation (Sec. III with more details in Appendixes A and B). The results we concentrate on here are the variation of the distribution function with the model parameters (Sec. IV), the I-V characteristics (Sec. V), and "heating" and "cooling" effects (Sec. VI).

II. N^+-N^--N^+ STRUCTURE: UNIVERSAL ASPECTS

The N^+-N^--N^+ structure (doping profile shown in inset to Fig. 1) has been intensively studied[5,6,18,19,25,27–31] as a simple, prototypical submicron structure. We idealize the experimental N^+-N^--N^+ GaAs structure[32] as a thin layer (0.4 μm) of lightly doped material ($N^- = 2\times 10^{15}$ cm^{-3}) between two slabs (2 μm wide each) of highly doped material ($N^+ = 10^{18}$ cm^{-3}). The scattering processes in the structure are modeled using relaxation times

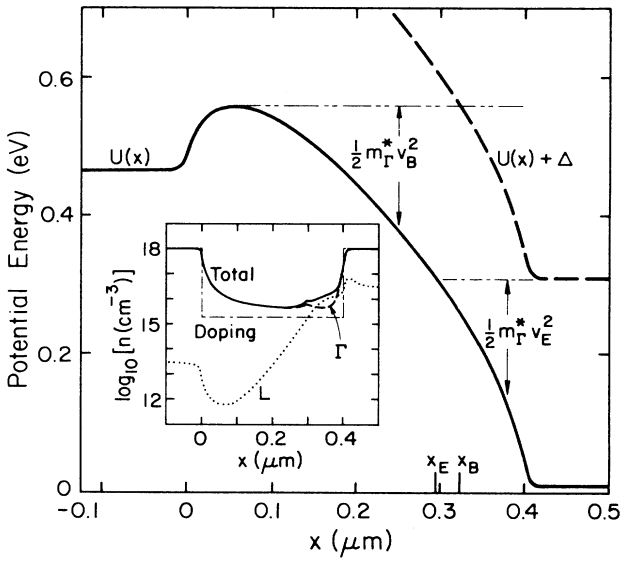

FIG. 1. The electron potential energy $U(x)$ (solid line) and $U(x)+\Delta$ ($\Delta = 0.3$ eV, dashed line) for $V_a = 0.47$ V and $T_0 = 300$ K within the two-valley model. Electrons injected over the potential maximum at $x_1 = 0.054$ μm are energetically able to transfer to the L valley once their energy lies above the dashed line. At $x_B = 0.323$ μm electrons with $v = v_B(x)$ can transfer to the L valley (intersection of dashed and double-dotted–dashed lines) where $v_B(x)$ is the minimum ballistic velocity defined by $m_\Gamma^* v_B^2(x)/2 = U(x_1) - U(x)$. Echo electrons created by $L \rightarrow \Gamma$ transfer have a minimum (absolute) velocity given by $m_\Gamma^* v_E^2(x)/2 = U(0.45\ \mu\text{m}) + \Delta - U(x)$, and reflect from the potential barrier near $x_E = 0.295$ μm. The inset shows the total electron density (solid line), $n_\Gamma(x)$ (dashed line), $n_L(x)$ (dotted line), and the doping profile (dotted-dashed line). $\Gamma \rightarrow L$ transfer causes a dramatic increase in the total charge for $0.3 \le x \le 0.4$ μm. In the actual calculation the structure extends from -2 μm to 2.4 μm to allow sufficient space for n_L to decay.

and can include intervalley processes. Typical potential energy and electric field profiles for the N^+-N^--N^+ are shown in Figs. 1 and 2, respectively. Note both the large inhomogeneities and the large built-in electric field near the doping steps. We can understand our previous results[7,26] in terms of general features of the potential profile. Below we summarize these results and indicate their universal nature.

The basic features of the potential profile in Fig. 1 are as follows. (i) There is a potential barrier at the left-hand N^+/N^- interface caused by spillover of electrons from the highly doped region into the lightly doped region. (ii) The potential drops sharply across the low-resistivity, submicron N^- region yielding a large electric field (≈ 10 kV/cm). (iii) At the right-hand N^+/N^- interface, $U(x)$ abruptly becomes nearly constant.

Conditions for ballistic electrons. When the mean free path, l, is large compared to the spatial scale on which $U(x)$ varies, ballistic electrons are generated. First, electrons are emitted thermionically[31] over the potential maximum at x_1 because the potential barrier both prevents electrons with $v<0$ from reaching x_1 and skims electrons with $v>0$ leaving them with an approximately Maxwellian distribution. The salient feature produced by skimming is an increase in $f(v,x_1)$ at $v=0$ (for example, see Fig. 3). Second, the $v>0$ electrons are accelerated by the high field in the N^- region. When the potential drops more than kT_0 within a mean free path, these electrons are accelerated to high velocities before scattering which creates a prominent ballistic-electron peak in the distribution function.

It is important to realize that the conditions described above for producing a ballistic-electron peak in the distribution function—a rapid change from a low field to a high field near the potential maximum followed by a potential drop of several kT_0 within a mean free path—are in fact present in several well-known structures in addition to the N^+-N^--N^+ discussed here. Examples include graded band-gap structures formed of $Al_xGa_{1-x}As$ and GaAs,[33] heterojunction transistor structures formed using $Al_xGa_{1-x}As$/GaAs interfaces,[34] and planar doped barrier structures.[35] Ballistic electrons have recently been observed in both the planar doped barrier[9] and the graded band-gap[10–12] structures.

Ballistic echoes. The presence of two valleys in the conduction band of GaAs can lead to "echoes" of the ballistic electrons; these echoes are generated in the region near the right-hand N^-/N^+ doping step by the rapid spatial decay of the high density of L-valley electrons. The combination of $\Gamma \rightarrow L$ and subsequent $L \rightarrow \Gamma$ transfer creates sharp new structure in $f_\Gamma(v,x)$, which we have called ballistic-electron echoes[26] (see Fig. 3 of Ref. 26 or Fig. 4 of this paper), by the following mechanism. (i) Electrons

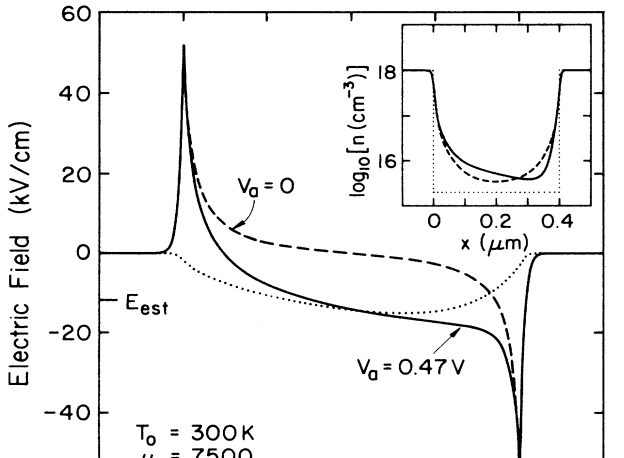

FIG. 2. The electric field profile for the N^+-N^--N^+ structure for two applied voltages ($V_a=0.47$ V for the solid line, $V_a=0.0$ V for the dashed line) using the one-valley, single-relaxation-time model. Large electric fields occur at both doping steps for both applied voltages. Subtracting the field for $V_a=0$ from that for $V_a=0.47$ (dotted line), we see that the applied field is largest in the high resistivity N^- region and is close to the field obtained by dividing the applied voltage by the length of the N^- region ($E_{est}=-11.8$ kV/cm). The inset shows the doping profile (dotted line) and the electron concentration for both applied voltages ($V_a=0.47$ V for the solid line, $V_a=0.0$V for the dashed line).

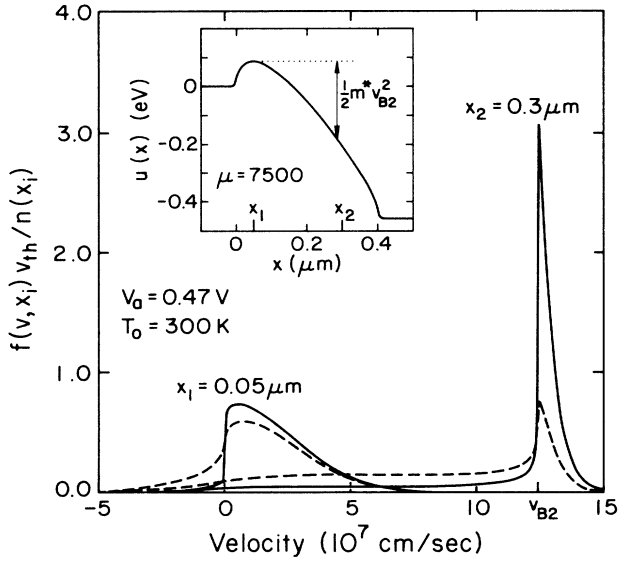

FIG. 3. Velocity distribution functions normalized by $n(x)/v_{th}$ ($T_0=300$ K, $v_{th}=2.6\times10^7$ cm/sec) at two points for two different mobilities in the N^- region [$\mu=40\,000$ cm^2/V sec (solid lines) and $\mu=7500$ cm^2/V sec (dashed lines)] within the single-valley model. The mobility in the N^+ regions is 7500 cm^2/V sec in both cases. At both points the higher mobility enhances the sharp ballistic structure of the distribution function. The inset shows the potential energy profile for the $\mu=7500$ cm^2/V sec case and indicates the two spatial points ($x_1=0.05$ μm, $x_2=0.3$ μm) for which the distributions are shown. The minimum ballistic velocity at point x_2 defined by $m^*v_{B2}^2/2=U(x_1)-U(x_2)$ falls on the sharp low-velocity edge of the peak in $f(v,x_2)$.

accelerated by the electric field in the N^- region transfer to the L valley, where they have a small kinetic energy because of the large effective mass and scattering rate. (ii) The small electric field in the N^+ region can no longer maintain the Γ-to-L density ratio of the N^- region thus causing a net flow of electrons from L to Γ. (iii) Electrons scattered from L are injected isotropically into Γ with kinetic energy greater than Δ, the L-Γ splitting. (iv) The $v<0$ electrons travel towards the barrier ballistically producing an echo peak, examples of which are shown in the $v<0$ region of Fig. 4. (v) At the turning point, near x_E, the electrons reflect from the potential barrier and return towards the N^+ region producing another echo peak for $v>0$.

The presence of echo peaks in the distribution function, like the presence of ballistic electrons, depends only on general features of the potential energy profile. First, a large density of L-valley electrons is needed; in a submicron structure the voltage drop [$U(x_1)$ in Fig. 1] must be greater than the energy difference between the valleys, Δ. Second, the electric field driving $\Gamma \rightarrow L$ transfer must abruptly end in order to allow intense $L \rightarrow \Gamma$ transfer. As we will see below, $L \rightarrow \Gamma$ transfer occurs within 0.05 μm

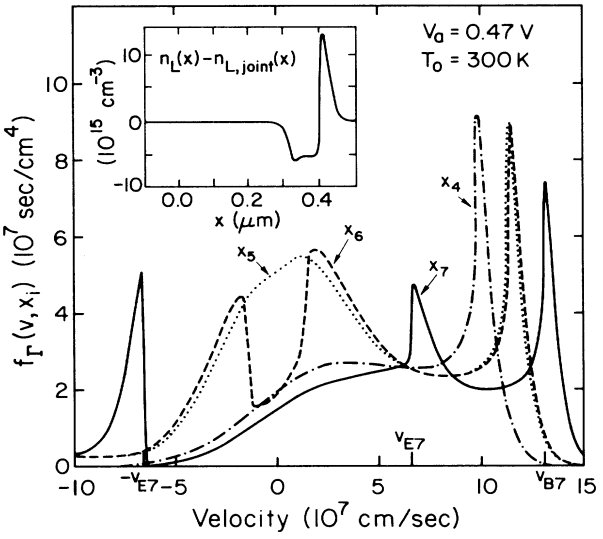

FIG. 4. Unnormalized velocity distributions for Γ-valley electrons showing formation of echo peaks. The distributions all show a prominent ballistic electron peak at large positive velocity as in the region before transfer to the L valley ($x_4=0.254$ μm, dotted-dashed line). At small velocity, the hump near $v=0$ present at $x_5=0.294$ μm (dotted line) splits into two ballistic electron echo peaks at $x_6=0.298$ μm (dashed line) and $x_7=0.34$ μm (solid line), one traveling with $v<0$, one with $v>0$. As the echo electrons are accelerated to more positive velocity, the magnitude of the peak, as indicated by the size of the sharp edge, decreases because of scattering out of the peak as the electrons travel towards the potential barrier ($v<0$) and back ($v>0$). The inset shows the difference in densities, $n_L(x)-n_{L,\text{joint}}(x)$, which drives $L \rightarrow \Gamma$ transfer. $\Gamma \rightarrow L$ transfer occurs when $n_L - n_{L,\text{joint}} < 0$ as in the region $0.3 \leq x \leq 0.4$ μm, while the strong $L \rightarrow \Gamma$ transfer for $0.4 \leq x \leq 0.45$ μm produces the echo peaks in the distribution function.

of the right-hand doping step (Fig. 4), thus the change in electric field must occur over a shorter distance. The well-known structures listed above as potential ballistic-electron structures should also show echo-electron effects.

Having presented a summary of the universal aspects of our previous work, we now present the models used in this work.

III. MODELS AND METHODS

We use the Boltzmann equation to calculate the distribution of electrons, $f(v,x)$, using two models for the collision term. First, we use a single-valley, single-relaxation-time model[7]—the simplest model possible, but one in which ballistic electrons are evident. Then we consider a two-valley, four-relaxation-time model[23,26] for GaAs that includes the most important band-structure effect within a one-dimensional approximation for the velocity dependence of the relaxation rates. While our use of relaxation times is not strictly valid for GaAs,[22] we feel these simple, structureless scattering models are useful for these preliminary investigations of inhomogeneous effects within the Boltzmann equation, in addition to making the problem tractable.

For either model, the stationary-state Boltzmann equation in terms of the electric field $E(x)$ and collision term $(\partial f/\partial t)_c$ is

$$-\frac{eE}{m_i^*}\frac{\partial f_i}{\partial v}+v\frac{\partial f_i}{\partial x}=\left[\frac{\partial f_i}{\partial t}\right]_c , \tag{1}$$

where i refers to the Γ or L valley in the two-valley model and is superfluous in the single-valley case. An effective mass characterizes each valley which are both assumed to be parabolic. The Boltzmann equation must be solved self-consistently with the Poisson equation for the electric field produced by the doping profile $N_D(x)$ and electron density $n(x)$

$$\frac{dE}{dx}=\frac{4\pi e}{\epsilon}[N_D(x)-n(x)] , \tag{2}$$

where ϵ is the static dielectric constant. The electron density is related to the distribution function by

$$n(x)=\int_{-\infty}^{\infty} dv f(v,x) . \tag{3}$$

In the single-valley model we assume that f relaxes to a local equilibrium (LE) distribution, $f_{\text{LE}}(v,x)$, at a rate τ^{-1} which is independent of energy or position. For the local equilibrium distribution we take a Maxwellian at the lattice temperature, T_0, normalized to the electron density,

$$f_{\text{LE}}(v,x)=n(x)\left[\frac{m^*}{2\pi kT_0}\right]^{1/2}\exp\left[-\frac{m^*v^2}{2kT_0}\right] . \tag{4}$$

Thus the collision term in the single-valley case is

$$\left[\frac{\partial f}{\partial t}\right]_c=-\frac{f(v,x)-f_{\text{LE}}(v,x)}{\tau} . \tag{5}$$

We wish to call attention to four features of this collision term. (i) The current continuity equation ($dJ/dx=0$) is

explicitly obeyed because we use the true electron density in normalizing f_{LE}. (ii) The average energy of the distribution $f(v,x)$ is not necessarily that of the distribution $f_{LE}(v,x)$; hence, the collisions are inelastic. (iii) The use of a Maxwellian distribution for $f_{LE}(v,x)$ is not strictly applicable to the degenerate N^+ regions. We note that our method could be extended to the degenerate case by using a Fermi-Dirac function for the local equilibrium distribution; however, we believe that this would only modify the barrier height and behavior in the N^+ regions slightly.[36] (iv) For a constant relaxation rate, the dependence of $f(v,x)$ on velocities perpendicular to the electric field factors out of the Boltzmann equation: f is simply a Maxwellian in the perpendicular velocities.

Turning now to the two-valley model, we can study within our Boltzmann equation approach transferred electron effects which are crucial in high-field transport in III-V materials.[37] Our model for GaAs (Refs. 23 and 26) includes two valleys in the conduction band of GaAs: the conduction-band minimum at Γ in the Brillouin zone and the next to lowest energy valley at L which is $\Delta=0.3$ eV above the Γ minimum.[38] While there are four degenerate L valleys in GaAs, we include only a single, generic "L valley."[39]

The electrons in each valley have a separate distribution function, $f_\Gamma(v,x)$ and $f_L(v,x)$, and electron density, $n_\Gamma(x)$ and $n_L(x)$. An intravalley and intervalley scattering process for each valley requires four relaxation times $\tau_{\Gamma\Gamma}$, $\tau_{\Gamma L}$, τ_{LL}, and $\tau_{L\Gamma}$ where the first (second) index indicates the valley from (to) which the electron scatters. Each process relaxes the electrons to a local equilibrium characterized by the lattice temperature T_0 and a chemical potential determined by particle-conservation conditions. We assume the $\Gamma\rightarrow\Gamma$ process conserves Γ electrons, the $L\rightarrow L$ process conserves L electrons, and the sum of the $\Gamma\rightarrow L$ and $L\rightarrow\Gamma$ processes conserves the total electron density. The chemical potential for the $\Gamma\rightarrow L$ and $L\rightarrow\Gamma$ processes is the same and provides the coupling between the two valleys. Thus the intervalley processes relax the electrons to an equilibrium between the two valleys, a joint local equilibrium.

Three relaxation times, $\tau_{\Gamma\Gamma}$, τ_{LL}, and $\tau_{L\Gamma}$, are taken to be constants, independent of energy; $\tau_{\Gamma L}$ and $\tau_{L\Gamma}$ are related by detailed balance. The $\Gamma\rightarrow L$ process turns on when $\Gamma\rightarrow L$ transfer is energetically possible. We assume a $\Gamma\rightarrow L$ scattering rate form,

$$\tau_{\Gamma L}^{-1}(v)=\tau_{\Gamma L}^{-1}\Theta(m_\Gamma^* v^2/2-\Delta)\ , \tag{6}$$

that depends only on the velocity parallel to the electric field; this reduces the problem to one dimension in velocity which is consistent with our neglect of L-valley degeneracy above. Note that as in the single-valley case, because τ^{-1} is independent of the velocity perpendicular to the field; f is simply a Maxwellian in the perpendicular velocity.

The basic equations for the two-valley model have been presented previously;[23,26] Appendix A contains a more detailed discussion than is available in either preceding work. We take three parameters in our model from experiment: $m_\Gamma^*=0.069m_e$, $\Delta=0.3$ eV, and $\mu_{\Gamma\Gamma}=e\tau_{\Gamma\Gamma}/m_\Gamma^*=7500$ cm^2/V sec which corresponds to $\tau_{\Gamma\Gamma}=2.9\times10^{-13}$ sec.[38,40] The remaining three parameters are set by fitting to the experimental velocity-field curve[23,40] in bulk GaAs for which our model is analytically soluble:[23,41] $m_L^*=1.2m_e$, $\tau_{\Gamma L}^{-1}/\tau_{\Gamma\Gamma}^{-1}=2$, and $(\tau_{LL}^{-1}+\tau_{L\Gamma}^{-1})/\tau_{\Gamma\Gamma}^{-1}=10.8$.[42] In the case of the single-valley model, we use the Γ-valley mass and $\tau_{\Gamma\Gamma}$ given above.

The solution of these models proceeds via numerical iteration [(1)–(5) for the single valley model[7]; details of our method can be found in Appendix B.

IV. VARIATION OF $f(v,x)$ WITH MOBILITY, TEMPERATURE, AND VOLTAGE

There are two parameters in the models described above which can easily be varied experimentally—the lattice temperature T_0 and the applied voltage V_a. However, before presenting our results for the effect of these two parameters on the distribution function $f(v,x)$, we discuss the role of the scattering parameter within the single-valley model, τ or the mobility $\mu=e\tau/m^*$, so as to demonstrate clearly the ballistic effects. In varying the mobility, we discovered that the mobility in the N^+ region has little effect on our results.[43] Hence we restrict ourselves here to varying the mobility in the N^- region (the mobility in the N^+ region is fixed at 7500 cm^2/V sec).

Effect of mobility. One expects, of course, that an increase in the mobility will lead to an enhancement of the ballistic effects. This expectation is borne out in Fig. 3 where we have plotted the distribution function at two different values of x and for two different mobilities in the N^- region (7500 cm^2/V sec and 40 000 cm^2/V sec). An increase in the mobility sharpens the distribution at the top of the potential barrier ($x_1=0.05$ μm) bringing it closer to the thermionic emission limit (a Maxwellian for $v>0$ and zero for $v<0$). Further down the structure at $x_2=0.3$ μm, the ballistic peak is larger for the higher mobility; 72% of the electrons at x_2 are in the ballistic peak for $\mu=40\,000$ cm^2/V sec compared to 24% for $\mu=7500$ cm^2/V sec.

Effect of temperature. The effect of varying the lattice temperature, T_0, within the single-valley model is shown in Fig. 5. By controlling the emission over the initial barrier at x_1, T_0 controls the width of the ballistic electron peak in energy—it is fixed at kT_0. Thus lowering the lattice temperature from 300 to 77 K results in a narrower ballistic electron peak (Fig. 5). Accompanying this narrowing of the ballistic peak is an increase in the height of the peak; however, the fraction of electrons in the ballistic peak at the point x_2 actually decreases as the temperature is lowered (from 0.24 at 300 K to 0.14 at 77 K) because of increased scattering near the potential maximum where the average velocity of electrons is lower for $T=77$ K (cf. pp. 85–87 of Ref. 36).

Variation near the echo turning point. The second easily varied parameter in the models is the applied voltage, V_a, and we will study the effects of V_a on $f_\Gamma(v,x)$ within the two-valley model in order to see the influence V_a has on the echo peaks. Throughout this work, we concentrate on changes in $f_\Gamma(v,x)$ rather than $f_L(v,x)$ because deviations of f_L from a drifted Maxwellian are very small (cf.

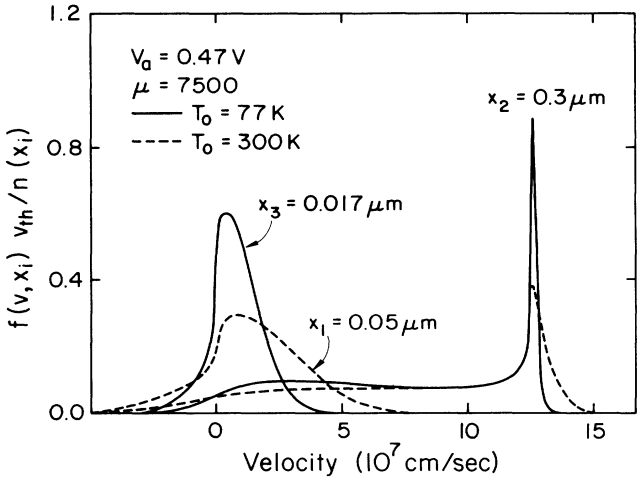

FIG. 5. Velocity distribution functions normalized by $n(x)/v_{\rm th}$ at two different temperatures. Distributions for $T_0=77$ K (solid lines) and for $T_0=300$ K (dashed lines) are compared at the maximum of the potential energy curve for each temperature (0.017 μm for $T_0=77$ K, 0.05 μm for $T_0=300$ K). The lower lattice temperature produces stronger but narrower ballistic peaks in the distribution function; however, the fraction of electrons which are ballistic is less for $T=77$ K (0.14) than for $T=300$ K (0.24) because of increased scattering near the potential maximum in the $T=77$ K case.

p. 178 of Ref. 36); in fact, even the temperature variation in the L valley is small—less than 8% for $V_a=0.47$ V at $T_0=300$ K. The basic mechanism for electron echoes was discussed previously[26] and reviewed above (Sec. II); however, before proceeding to the dependence of f_Γ on V_a, we present in Fig. 4 a detail of $f_\Gamma(v,x)$ near the echo-electron turning point $x_E=0.295$ μm, the point where echo electrons are reflected to move in the positive-x direction. To the left of the echo-electron turning point ($x_4=0.254$ μm $<x_E$), the distribution looks surprisingly like the single-valley distribution, whereas far to the right of the turning point ($x_7=0.34$ μm $>x_E$) $f(v,x)$ has the classic three-peak echo form.[26] At $x=x_7$, 14% of the electrons are in the echo peaks compared to 11% in the ballistic peak. For x only slightly to the left of x_E ($x_5=0.294$ μm $\leq x_E$) the echo electrons with greater than the minimum energy spill over and cause a hump in f around $v=0$. In contrast, for x slightly to the right of x_E ($x_6=0.298$ μm $\geq x_E$) the two echo peaks have just formed. The sharp edges of the echo peaks are caused by the sharp turn-on of the $\Gamma\rightarrow L$ transfer within our model [Eq. (6)]; these sharp edges fall at the velocities $\pm v_E(x)$ where

$$m_\Gamma^* v_E^2(x)/2 = U(0.45\ \mu\text{m}) + \Delta - U(x)\ . \tag{7}$$

The size of the discontinuity in f_Γ at the echo velocity is a measure of the quantity of echo electrons. The decrease in the echo discontinuity as the electrons travel towards the barrier ($v<0$) and away ($v>0$) shows that scattering of the echo electrons does take place.

Our explanation for the formation of echo peaks suggests that the $L\rightarrow\Gamma$ transfer occurs very close to the right-hand N^-/N^+ step. To verify this point, we show in the inset to Fig. 5 the density difference which drives $L\rightarrow\Gamma$ transfer, $n_L(x)-n_{L,\rm joint}(x)$ [see Eqs. (A1) and (A4)]. The negative value of this quantity for $0.3\leq x\leq 0.4$ μm indicates $\Gamma\rightarrow L$ transfer while its large positive value for $0.4\leq x\leq 0.45$ μm indicates particularly intense $L\rightarrow\Gamma$ transfer in this narrow region. We believe, therefore, that the echo-electron peaks are formed in the region $0.4\leq x\leq 0.45$ μm and that the transition from high-field to low-field region must occur in a distance less than 0.05μm in order to produce echoes.

Effect of voltage. Turning now to the effect of the applied voltage on $f(v,x)$, we expect that an increase in V_a should enhance both the ballistic peak (increased acceleration) and the echo peaks (more $\Gamma\rightarrow L$ transfer resulting in more $L\rightarrow\Gamma$ transfer). The distributions shown in Fig. 6 bear out these expectations. Indeed, the echo peaks are particularly dramatic at high voltage where the large barrier to electrons diffusing from the N^+ region depresses the number of electrons with $v\approx 0$. In contrast, at low voltages the Maxwellian distribution of electrons diffusing from the N^+ into the N^- region dominates the distribution. Also note in the high-voltage distribution function a discontinuity in the derivative of f at $\pm v_c=(2\Delta/m_\Gamma^*)^{1/2}$ caused by intervalley transfer as in the homogeneous field case.[23]

Ballistic electrons. The importance of ballistic electrons in the distribution functions shown in this section demands further characterization of this part of the distribution. To do this, we define $n_B(x)$ to be the density of

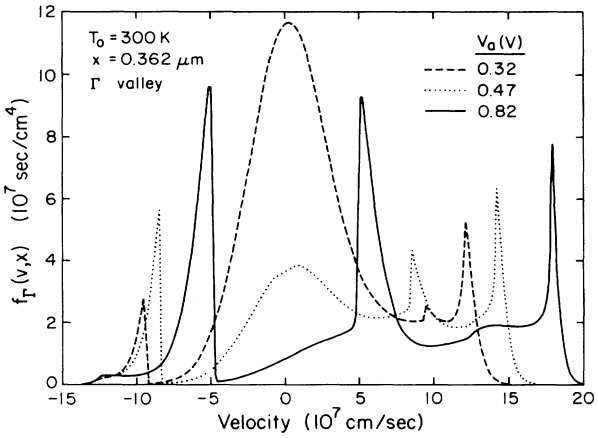

FIG. 6. Unnormalized velocity distributions for Γ-valley electrons at $x=0.36$ μm for three applied voltages ($V_a=0.32$ V, dashed line; $V_a=0.47$ V, dotted line; and $V_a=0.82$ V, solid line). A larger applied voltage enhances both the ballistic and the echo peaks. It causes the ballistic peak to move to higher velocity. In contrast, it moves the echo peaks towards $v=0$ because the potential energy, $U(x)$, increases while the initial energy of the echo electrons remains fixed at approximately the energy separation of the Γ and L valleys. In addition, the increase in $U(x)$ with larger applied voltage inhibits the diffusion of thermal electrons from the right-hand N^+ region, causing the Maxwellian part of the distribution function near $v=0$ to decrease.

those (Γ valley) electrons with $v>0$ and with energy greater than the maximum of the potential energy curve $U_{\max}=U(x_1)$ (Fig. 1). Once a ballistic peak has formed ($x>x_1$), $n_B(x)$ is the density of ballistic electrons, while for $x<x_1$, $n_B(x)$ is simply the density of electrons which are energetically able to surpass the potential barrier. Figure 7 shows $n_B(x)$ for both the single and two-valley models at $T_0=300$ K and $V_a=0.47$ V. Also in Fig. 7 we plot $n_B(x)/n(x)$ which downstream from the potential maximum gives the fraction of electrons which are ballistic.

The curves of $n_B(x)$ in Fig. 7 for the single-valley and two-valley models are surprisingly similar in both shape and magnitude. The main deviation occurs once transfer to the L valley becomes significant in the right-hand portion of the N^- region. The point x_B, defined in Fig. 1 to be the point at which the electrons in the entire ballistic peak become energetically able to transfer to the L valley, gives a good estimate of where $n_B(x)$ for the single-valley model starts to deviate from $n_B(x)$ for the two-valley model. There are additional small deviations for $x<x_1$ caused by the quicker decay of $f(v)$ in the two-valley case for $v>(2\Delta/m_\Gamma^*)^{1/2}$ (cf. pp. 171–175 of Ref. 36). The plots of the fractional effect show that in both models a significant fraction of the electrons is ballistic.

V. *I-V* CHARACTERISTICS AND AVERAGE VELOCITY

Having calculated the distribution functions for several sets of parameters for both scattering models as reported in the preceding section, we can now perform averages over these distributions to find other quantities of interest, such as the current and average velocity. The current density is given by

$$I=-e\int dv v f(v,x)\ , \tag{8}$$

which is closely related to the average velocity,

$$\bar{v}(x)=-I/en(x)\ . \tag{9}$$

Because our collision integrals conserve particle number, I as defined above should not depend on x; in fact, our calculational method (see Appendix B) results in less than 1% variation of I in the single-valley case and about 4% variation in the two-valley case. Figure 8 shows the I-V curves for the single-valley model for two mobilities of the N^- region at each of two temperatures, the I-V curve for the two-valley model at 300 K, and the experimental I-V curve at both temperatures.[32]

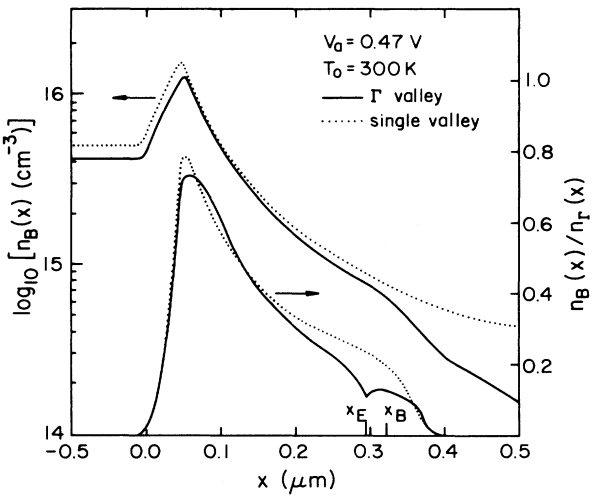

FIG. 7. The logarithm of the density, $n_B(x)$, of those (Γ-valley) electrons with total energy greater than the maximum of the potential energy and the ratio of this density to the total density for both the two-valley (solid lines) and single-valley (dotted lines) models. For x downstream from the potential maximum, $x>x_1$ (x_1 defined in Fig. 1), $n_B(x)$ is the density of ballistic electrons, while for $x<x_1$, $n_B(x)$ is the density of electrons which are energetically able to be injected over the barrier. The surprising similarity in shape and magnitude of the single-valley and two-valley results indicates that the single-valley calculation provides a good estimate of the size of ballistic electron effects. Deviations occur for $x>x_B$ (where x_B is defined in Fig. 1) because the entire ballistic peak becomes able to scatter to the L valley at this point. The fraction of electrons which are ballistic is significant for both models, the greatest deviation occurring near the echo turning point x_E (defined in Fig. 1).

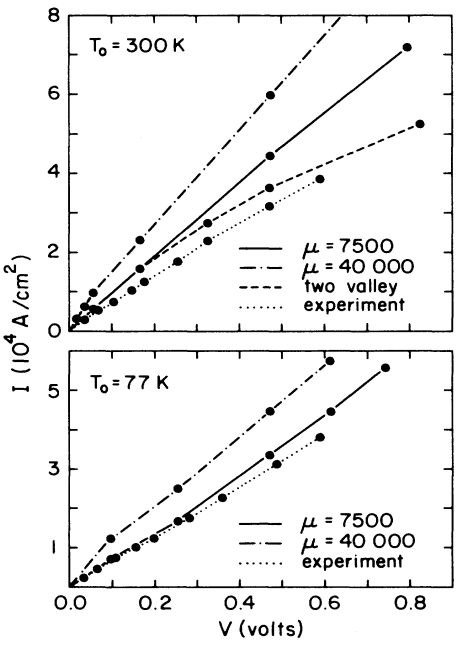

FIG. 8. Comparison of the experimental (Ref. 32) I-V characteristics to those calculated for the one-valley model at two temperatures and two mobilities and for the two-valley model at $T_0=300$ K. At 300 K (top panel) the experimental curve (dotted line) lies below both the two one-valley results ($\mu=7500$ cm^2/V sec, solid line; $\mu=40\,000$ in the N^- region, dotted-dashed line) and the two-valley result (dashed line). All the curves are nearly linear over the entire voltage range, and the current is not greatly affected by either the temperature or mobility. Use of the two-valley model improves agreement between theory and experiment for applied voltages where transfer to the L valley is important ($V_a\geq 0.2$ V).

Several features of the curves in Fig. 8 require comment. (i) The most striking feature is that all of the curves are nearly linear despite the dramatic structure in the distribution. This disappointing property of the N^+-N^--N^+ structure indicates that the current is determined by boundary effects—essentially by emission over the barrier[31]—rather than by effects in the region where the distribution function has structure. (ii) The theory for the two-valley model showed improved agreement with experiment. In the results of the two-valley model there is a small change in slope of the I-V curve starting at about 0.2 V. This corresponds to the applied voltage needed to initiate transfer, $V_{a,\text{transfer}}$,

$$V_{a,\text{transfer}} \approx \Delta - [U(x_1) - U(0)] , \tag{10}$$

where the term in square brackets approximates the barrier height seen by the electrons coming from the left. (iii) The value of T_0 does not have a large effect on the current. This result while initially surprising for emission over a barrier follows simply from the fact that the barrier height, ϕ_B, scales with T_0 since ϕ_B itself depends on spillover of electrons from the N^+ into the N^- region. In fact, ϕ_B at 300 K is 0.086 V while at 77 K, ϕ_B is 0.018 V. (4) Neither does the value of the mobility affect the current greatly. This is related to a small change in the barrier heights; ϕ_B decreases by only 2% when the mobility of the N^- region changes from 7500 cm^2/V sec to 40 000 cm^2/V sec.

To illustrate this latter effect, we plot in Fig. 9 the current versus the mobility in the N^- region (the mobility in the N^+ region is fixed throughout at 7500 cm^2/V sec) for two applied voltages in the single-valley model. At low mobilities, I scales linearly with μ as one would expect based on bulk behavior ($I = -en\mu E$). However, for both voltages, the current saturates at high mobilities. That is, the current becomes insensitive to the material properties of the N^- region in the ballistic regime, presumably because the current is controlled by boundary effects such as emission over the initial barrier.

The average velocity at $T_0 = 300$ K and $V_a = 0.47$ V for both the single-valley model and the two-valley model is shown in Fig. 10. For the two-valley case, the contribution of each valley is shown, $\bar{v}_\Gamma(x)$ and $\bar{v}_L(x)$. In the highly nonequilibrium situation considered here, it is not surprising that both the single-valley result and the average velocity in the Γ valley exceed the thermal velocity, $v_{\text{th}} = (kT_0/m^*)^{1/2} = 2.6 \times 10^7$ cm/sec, by a substantial amount. Once substantial transfer takes place ($x > x_B$, x_B defined in Fig. 1), the very small value of $\bar{v}_L(x)$, due to both the higher effective mass and the higher scattering rate in the L valley, produces a sharp drop in $\bar{v}(x)$ for the two-valley model. The sharp dip in $v_\Gamma(x)$ near the echo electron turning point (x_E) results from the substantial number of slow moving echo electrons near this point.

VI. "HEATING" AND "COOLING"

It is clear from the distributions plotted in Figs. 3–6 that the width of the velocity distributions varies greatly across the structure. This width of $f(v,x)$ can be easily

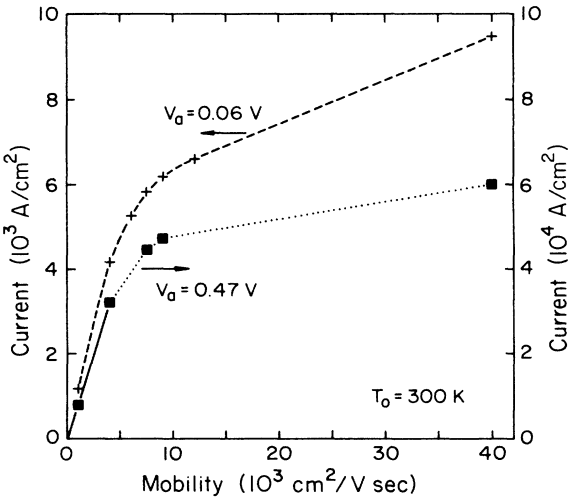

FIG. 9. The current as a function of the mobility in the N^- region for two applied voltages ($V_a = 0.47$ V, dots, and $V_a = 0.06$ V, pluses). The mobility in the N^+ regions is fixed at 7500 cm^2/V sec. For low mobilities, the current varies linearly with mobility, as expected from the result for a uniform system, $I = -enE\mu$. At higher mobilities, the current saturates, becoming insensitive to the value of the mobility in the submicron region. The higher applied voltage enhances the insensitivity of I to μ because boundary effects become more important as the electron velocity increases.

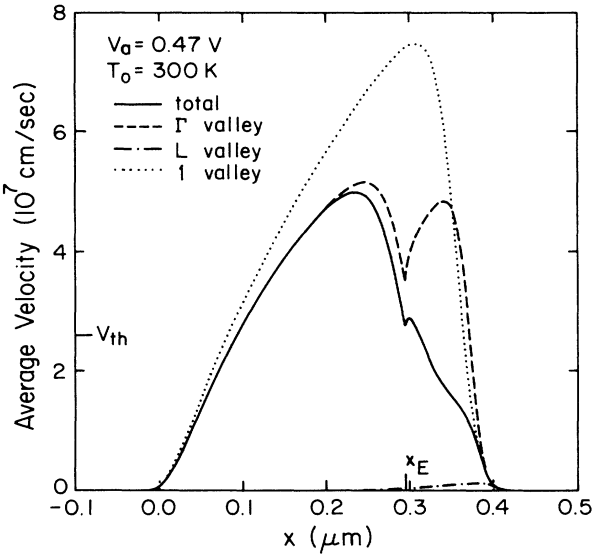

FIG. 10. The average velocity as a function of distance at $V_a = 0.47$ V for all electrons (solid line), the Γ-valley electrons (dashed line), and the L-valley electrons (dotted-dashed line) compared to the single-valley result (dotted line). The large effective mass and scattering rate in the L valley cause the average velocity of L-valley electrons to be small. Thus, when substantial transfer to the L valley occurs, the total average velocity decreases dramatically. The velocity of Γ electrons dips sharply near $x_E = 0.295$ μm, the point where echo electrons reflect from the potential barrier.

calculated from an average of $f(v,x)$, much as the average velocity was in the preceding section, and is closely related to the average energy. The structure in the distribution functions in Figs. 3–6 shows clearly that no thermodynamic temperature exists for these systems since a drifted-Maxwellian distribution[17] is not a good approximation. However, it seems reasonable to study the width of the distribution by expressing it as a temperature, $T^*(x)$,

$$kT^*(x)=m^*\langle(v-\bar{v})^2\rangle \ . \tag{11}$$

Figure 11 shows $T^*(x)$ for several voltages and two mobilities within the single-valley model.

First, at the lowest voltage, $T^*(x)-T_0$ varies quite significantly and is nearly antisymmetric about the middle of the N^- region, $x=0.2$ μm. This indicates that heating (and cooling) here is a first-order effect in the applied voltage (or current) rather than the well-known quadratic dependence of T^* on E (or current) in bulk material. In fact, heating is generally first order in an inhomogeneous system as seen by the following argument. The power input by the field is

$$P=JE=-en\bar{v}(x)E(x) \ . \tag{12}$$

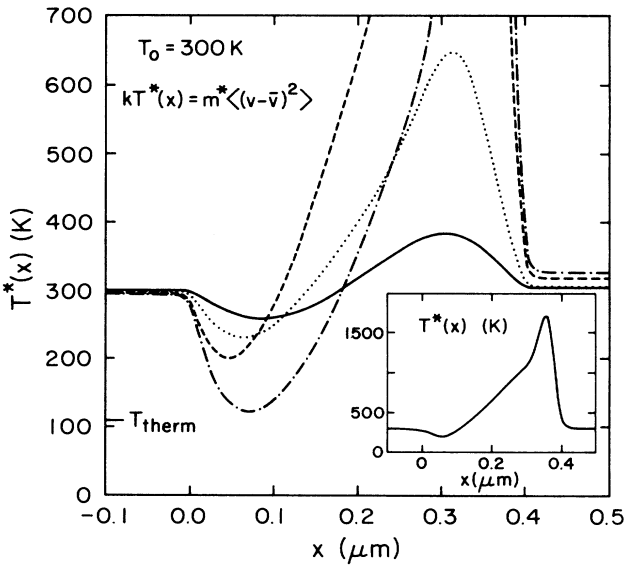

FIG. 11. The "temperature" as a function of distance defined as the width of the distribution, $kT^*(x)=m^*\langle(v-\bar{v})^2\rangle$, for three applied voltages and two mobilities within the single-valley model. Even at the lowest applied voltage ($V_a=0.06$ V, $\mu=7500$ cm^2/V sec, solid line), the built-in electric field (Fig. 2) "cools" and "heats" the electrons indicating that "heating" and "cooling" in an inhomogeneous structure are first order in the applied voltage. At higher voltages with the same mobility [$V_a=0.17$ V (dotted line), and $V_a=0.47$ V (dashed line)] $T^*(x)$ becomes asymmetric, the heating being much larger than the cooling. For a mobility of 40 000 cm^2/V sec in the N^- region ($V_a=0.47$ V, dotted-dashed line), the width of the distribution function approaches the thermionic emission limit [$T^*=110$ K, see Eq. (13)] at the top of the potential barrier. The inset shows the full $T^*(x)$ for $V_a=0.47$ V and $\mu=7500$ cm^2/V sec.

In an inhomogeneous system there is a built-in, nonzero field even when the applied voltage V_a is zero. Thus the leading order in the power, or heating, comes from the first-order dependence of $\bar{v}$ on V_a. The nearly antisymmetrical nature of $T^*(x)$ in our case comes from the antisymmetrical nature of the field for $V_a=0$ as shown in Fig. 2.

At higher voltages, $T^*(x)$ becomes very asymmetric—the width of the distribution in the region where there is a ballistic electron peak is very large. At the larger mobility ($\mu=40\,000$ cm^2/V sec in the N^- region) changes in $T^*(x)$ become even more dramatic. At the top of the potential barrier, $T^*(x)$ approaches the thermionic limit; for a large V_a and a long mean free path, the distribution should be Maxwellian for $v>0$ and zero for $v<0$ so that

$$T_{\text{therm}}=\frac{m^*}{k}(\overline{v^2}-\bar{v}^2)=T_0\left[1-\frac{2}{\pi}\right]\approx 110 \text{ K} \ . \tag{13}$$

is reached in the limit of large applied voltage.

VII. CONCLUSION

In this work we have presented results of a Boltzmann equation calculation of the distribution function in a N^+-N^--N^+ structure. The structure in the distribution function evident in our case—a ballistic peak and echo peaks—should be present in other small devices because, we argue, such structure depends only on general features of the potential energy profile. The necessary conditions for the ballistic peak are a rapid change from a low field to a high field near the potential maximum followed by a drop of several kT_0 within a mean free path; for the ballistic electron echoes, one must have a large density of L-valley electrons in a region where the electric field abruptly decreases.

As a function of the basic model parameters (μ, T, and V_a), the features of the distribution scale in the expected way: the peaks are enhanced by a higher mobility or applied voltage and narrow as the temperature is decreased. We should note at this point that the one-dimensional nature of our model undoubtedly enhances the echo effects; in a three-dimensional model the current traveling back towards the potential barrier is smaller than in the one-dimensional case. The distribution functions calculated for different applied voltages show, however, that a larger applied voltage greatly enhances the echo peaks. While there is a suggestion of echo effects in a three-dimensional Monte-Carlo Calculation,[30] the large size of the effect in the present one-dimensional case suggests that a further investigation in three dimensions would be highly rewarding.[44] Another weakness of our model is its neglect of electron-electron scattering—all collisions in our model bring the electrons towards an equilibrium with the lattice. In the lightly doped region considered here, we expect that this neglect is not serious; however, in more heavily doped material other effects such as plasmon emission[9] or electron-electron scattering[45] will be important and may broaden the distribution.

Despite the presence of the ballistic and echo peaks in the distribution function, the I-V characteristic for all cases considered here is linear. The plot of the current

versus mobility (Fig. 9) shows, however, that the N^+-N^--N^+ is not a simple resistor since the current becomes independent of mobility at large mobility.

Finally, heating and cooling in the N^+-N^--N^+ are first order in the applied field, a result which should be valid for all structures with built-in fields. Thus, any approach which neglects thermal gradient effects, such as the drift-diffusion equation, will fail in describing the linear response. In fact, in our earlier work where drift diffusion and Boltzmann equation results were compared for the same scattering model, the drift-diffusion equation over-estimated the current by about a factor of 2 for all applied voltages.[7] For larger applied voltages, the terms heating and cooling cannot be applied in their thermodynamic sense since the distribution function deviates so strongly from a drifted-Maxwellian distribution. However, it is clear that the width of the distribution varies dramatically across the structure, being smaller than the equilibrium width near the top of the potential barrier and larger than the equilibrium width throughout much of the N^- region.

ACKNOWLEDGMENTS

We appreciate many valuable discussions with J. H. Davies, N. D. Mermin, and C. J. Stanton. This work was supported by the U.S. Office of Naval Research under Contract No. N00014-80-C-0489.

APPENDIX A

In this appendix we specify in detail the two-valley model described briefly in Sec. III. Our approach has three key ingredients. (i) The Γ-valley and L-valley electrons are treated as separate species each described by a distribution function, $f_\Gamma(v,x)$ or $f_L(v,x)$. (ii) Both intravalley and intervalley scattering are modelled as relaxation to local equilibrium functions. (iii) Particle-conservation conditions determine the chemical potentials in the local equilibrium functions, and indeed how many independent chemical potentials there are.

The collision integral for the single-valley case [Eq. (5)] is replaced by two collision integrals, one for f_Γ and one for f_L as follows,

$$\left[\frac{\partial f_\Gamma}{\partial v}\right]_c = -\frac{f_\Gamma - f_{\Gamma,\mathrm{LE}}}{\tau_{\Gamma\Gamma}} - \frac{f_\Gamma - f_{\Gamma,\mathrm{joint\,LE}}}{\tau_{\Gamma L}} , \tag{A1a}$$

$$\left[\frac{\partial f_L}{\partial v}\right]_c = -\frac{f_L - f_{L,\mathrm{LE}}}{\tau_{LL}} \frac{f_L - f_{L,\mathrm{joint\,LE}}}{\tau_{L\Gamma}} . \tag{A1b}$$

The local equilibrium functions can be simply expressed as Fermi functions with respect to appropriate chemical potentials. Because the $\Gamma \rightarrow \Gamma$ process conserves the number of Γ electrons, the $L \rightarrow L$ process conserves the number of L electrons, and the intervalley processes conserve the total number of electrons, we use three independent chemical potentials: $\mu_\Gamma(x)$, $\mu_L(x)$, and $\mu_{\mathrm{joint}}(x)$ for the $\Gamma \rightarrow \Gamma$, $L \rightarrow L$, and intervalley processes, respectively. In terms of these chemical potentials, the local equilibrium functions as a function of k and x are

$$f_{i,\mathrm{LE}}(k,x) = \{1 + \exp[\varepsilon_i(k) + U(x) - \mu_i(x)]/kT_0\}^{-1} , \tag{A2a}$$

$$f_{i,\mathrm{joint\,LE}}(k,x) = \{1 + \exp[\varepsilon_i(k) + U(x) - \mu_{\mathrm{joint}}(x)]/kT_0\}^{-1} , \tag{A2b}$$

where

$$\varepsilon_i = \frac{\hbar^2 k^2}{2m_i^*} + \delta_{i,L}\Delta$$

and $i = \Gamma$ or L throughout.

We have assumed that the chemical potential is the same for both intervalley processes in order to mimic relaxation of the electrons to the joint equilibrium state of both the Γ and L valleys. (In the Γ valley, only electrons with energy large enough to transfer to L are involved as only these electrons can "communicate" with L.) This assumption is a reasonable one for intervalley scattering since any such process should act (roughly) to partition the electrons between the two valleys according to a local equilibrium. Notice that our assumption is not equivalent to assuming that $\tau_{\Gamma L}^{-1}$ mimics a $\Gamma \rightarrow L$ scattering rate, for in that case $f_{L,\mathrm{joint\,LE}}$ would depend only on the distribution of Γ-valley electrons while $f_{\Gamma,\mathrm{joint\,LE}}$ would depend only on the properties of L-valley electrons. In contrast, in our case both joint local equilibrium functions depend on the distributions in both valleys as will be made explicit below [Eq. (A15)].[46]

In the case of nondegenerate statistics considered in this paper, the local equilibrium functions considered in (A2) can be expressed (as a function of v and x) as a density times a normalized Maxwellian, $f_i^M(v)$

$$f_i^M(v) = \left[\frac{m_i^*}{2\pi kT_0}\right]^{1/2} \exp\left[-\frac{m_i^* v^2}{2kT_0}\right], \quad i = \Gamma, L , \tag{A3}$$

where the density is related to the chemical potential. For example, for the intervalley processes we have

$$f_{i,\mathrm{joint\,LE}}(v,x) = n_{i,\mathrm{joint}}(x) f_i^M(v) , \tag{A4}$$

where

$$n_{i,\mathrm{joint}}(x) = \exp[\mu_{\mathrm{joint}}(x) - U(x) - \Delta\delta_{i,L}]/kT_0 \times (2\pi kT_0 m_i^*)^{1/2}/\hbar . \tag{A5}$$

The fact that $\mu_{\mathrm{joint}}(x)$ is the same for both $n_{\Gamma,\mathrm{joint}}(x)$ and $n_{L,\mathrm{joint}}(x)$ implies that their ratio is the same as the ratio of the (global) equilibrium densities, $n_\Gamma^0(x)$ and $n_L^0(x)$, which we will call β,

$$\beta = \frac{n_{\Gamma,\mathrm{joint}}(x)}{n_{L,\mathrm{joint}}(x)} = \frac{n_\Gamma^0(x)}{n_L^0(x)} = \left[\frac{m_\Gamma^*}{m_L^*}\right]^{1/2} \exp\left[\frac{\Delta}{kT_0}\right] . \tag{A6}$$

In this equation, by using the square root of the masses and neglecting the degeneracy of the L valley, we have specialized to the one-dimensional, single-L-valley case considered in this paper and our previous work.[23,26]

A particle-conservation condition determines the value of each chemical potential. Thus our use of three independent chemical potentials above requires three-particle conservation conditions. First, the number of Γ

electrons is conserved by the $\Gamma \rightarrow \Gamma$ process. This and an analogous requirement for the L valley yield

$$\int_{-\infty}^{\infty} dv \frac{f_i - f_{i,\mathrm{LE}}}{\tau_{ii}} = 0, \quad i = \Gamma, L \ . \tag{A7}$$

In the intervalley terms, the chemical potential characterizing the two local equilibrium functions is set by conservation of total particle number,

$$\int_{-\infty}^{\infty} dv \sum_{\substack{i,j=\Gamma,L \\ (j \neq i)}} \frac{f_i - f_{i,\text{joint LE}}}{\tau_{ij}} = 0 \ . \tag{A8}$$

As noted in Sec. III, for an easily solved model, we choose $\tau_{\Gamma\Gamma}$, τ_{LL}, and $\tau_{L\Gamma}$ to be constant. The rate $\tau_{\Gamma L}^{-1}$ turns on when electrons are energetically able to transfer from Γ to L; we take $\tau_{\Gamma L}^{-1}(v) = \tau_{\Gamma L}^{-1} \Theta(m_{\Gamma}^{*} v^2/2 - \Delta)$ where v is the velocity parallel to the electric field and Θ is the step function. With this choice for the τ's, (A7) implies that

$$f_{i,\mathrm{LE}}(v,x) = n_i(x) f_i^{M}(v), \quad i = \Gamma, L \ . \tag{A9}$$

Now we must use (A8) and (A6) to solve for $n_{\Gamma,\text{joint}}(x)$ and $n_{L,\text{joint}}(x)$ in terms of f_Γ and f_L. To simplify the notation, we introduce the density, $n_{\Gamma}^{>}(x)$, of Γ-valley electrons which are energetically able to transfer to L

$$n_{\Gamma}^{>}(x) = \int dv \Theta(\varepsilon - \Delta) f_{\Gamma}(v,x) \ , \tag{A10}$$

and the equilibrium ratio, α, of this density to $n_\Gamma(x)$,

$$\alpha \equiv \frac{n_{\Gamma}^{>,0}(x)}{n_{\Gamma}^{0}(x)} = \int dv \, \Theta(\varepsilon - \Delta) f_{\Gamma}^{M}(v) = \mathrm{erfc}[(\Delta/kT_0)^{1/2}] \ . \tag{A11}$$

With this notation, (A8) becomes

$$\frac{n_{\Gamma}^{>}(x) - \alpha n_{\Gamma,\text{joint}}(x)}{\tau_{\Gamma L}} + \frac{n_L(x) - n_{L,\text{joint}}(x)}{\tau_{L\Gamma}} = 0 \ . \tag{A12}$$

The relation (A6) between $n_{\Gamma,\text{joint}}(x)$ and $n_{L,\text{joint}}(x)$ leads to

$$n_{L,\text{joint}}(x) = \frac{n_L(x) + n_{\Gamma}^{>}(x)\tau_{L\Gamma}/\tau_{\Gamma L}}{1 + \alpha\beta\tau_{L\Gamma}/\tau_{\Gamma L}} \ . \tag{A13}$$

Equation (A13) provides an expression for $n_{L,\text{joint}}(x)$ in terms of simple integrals over the distribution functions. However, because there is no independent experimental information for $\tau_{L\Gamma}$, we eliminate this additional free parameter by relating $\tau_{L\Gamma}$ to $\tau_{\Gamma L}$ using detailed balance. Within the relaxation-time approximation, detailed balance is of questionable validity and should not be used when information about $\tau_{L\Gamma}$ becomes available. A relation between global equilibrium quantities, detailed balance requires that the applied voltage be zero. Since, the relaxation times we use are independent of the field, it is easy to assume that the relation between $\tau_{L\Gamma}$ and $\tau_{\Gamma L}$ derived from detailed balance applies at all applied voltages.

Detailed balance in the intervalley processes simply states that in equilibrium the number of electrons transferring from the L valley to the Γ valley is equal to the number transferring from Γ to L:

$$\frac{n_L^0}{\tau_{L\Gamma}} = \frac{n_{\Gamma}^{>,0}}{\tau_{\Gamma L}} = \frac{\alpha n_{\Gamma}^{0}}{\tau_{\Gamma L}} \ . \tag{A14}$$

Used in the expression for $n_{L,\text{joint}}(x)$ (A13), (A14) implies

$$n_{L,\text{joint}}(x) = \tfrac{1}{2}[n_L(x) + n_{\Gamma}^{>}(x)/\alpha\beta] \ , \tag{A15a}$$

$$n_{\Gamma,\text{joint}}(x) = \tfrac{1}{2}[n_{\Gamma}^{>}(x)/\alpha + \beta n_L(x)] \ , \tag{A15b}$$

which are the expressions we use in solving the Boltzmann equations. This completes our discussion of the two-valley model; Eqs. (A1), (A3), (A4), (A9), and (A15) completely specify the model.

APPENDIX B

In this appendix we describe the method used to solve the coupled Boltzmann equation [Eq. (1)] and Poisson equation [Eq. (2)] in the N^+-N^--N^+ structure. We start by describing the procedure for the single-valley model and then present the changes necessary for the two-valley model. Since our method is iterative in the density, it is convenient to call the input and output of the ith iterate $n_i^{\text{in}}(x)$ and $n_i^{\text{out}}(x)$, respectively.

The basic procedure used in the single-valley case follows; each point in the outline is then discussed in a section of this appendix. (i) Guess an initial density $n_1^{\text{in}}(x)$ and generate f_{LE} and $E(x)$. (ii) Change variables in the Boltzmann equation from x and v to x and the total energy $w = v^2/2m^* + U(x)$. (iii) Solve the resulting set of independent ordinary differential equations on a grid in energy and space. For boundary values of f at the edge of the structure, use the solution[7,23] for a homogeneous field E_0 where E_0 is taken to be the boundary value of $E(x)$ calculated in step (i). (iv) Obtain an output density, $n^{\text{out}}(x) = \int dv f(v,x)$. (v) Scale $n^{\text{out}}(x)$ to maintain total charge neutrality. (vi) Use a simple screening procedure to damp charge oscillations and hence improve convergence. (vii) Finally, mix 1%–5% of $n_i^{\text{out}}(x)$ with $n_i^{\text{in}}(x)$ to generate the next initial density and from that the field $E(x)$, and local equilibrium distribution, f_{LE}. Steps (iii)–(vii) are repeated until the desired degree of convergence is achieved (typically a few hundred times).

Guess an initial density. We obtain our initial guess for the density of electrons and simultaneously for the electric field from the drift-diffusion equation within the single-relaxation-time approximation. Taking $\mu = e\tau/m^*$ and using the Einstein relation $D/\mu = kT_0/e$ to relate D to the lattice temperature, T_0, we obtain the following drift-diffusion equation,

$$J_{\mathrm{DD}} = \frac{e^2\tau}{m^*} n(x) E(x) + e\tau \frac{kT_0}{m^*} \frac{dn}{dx} \ . \tag{B1}$$

Equation (B1) is solved self-consistently with the Poisson equation [Eq. (2)] for $n(x)$ and $E(x)$ using a finite-difference method. As boundary conditions we fix the current J_{DD} at the desired value and set the density equal to N^+ at the edges of the structure. The spatial mesh used here and throughout this work concentrates points near the doping steps [by using the transformation $z = a \sinh(ax)$] and uses about 500 points.

Change variables in the Boltzmann equation. Given our

initial guesses for $f_{\rm LE}$ and $E(x)$, the Boltzmann equation becomes a first-order linear equation for $f(v,x)$ allowing us to use the method of characteristics[47] to transform the Boltzmann equation to a family of ordinary differential equations. This method is equivalent to changing variables from the usual x and v to x and the total electron energy, $w = v^2/2m^* + U(x)$. Because the velocity squared appears in the expression for w, the variables x and w do not fully specify the distribution function as the information about the sign of v is lost. We therefore introduce a new index, letting $f_+(w,x)$ be the distribution of electrons with $v>0$ and $f_-(w,x)$ be the distribution with $v<0$. Transforming Eq. (1) to the variables w and x gives

$$\pm v(w,x)\frac{df_\pm(w,x)}{dx} = -\frac{f_\pm(w,x)-f_{\rm LE}(w,x)}{\tau} , \quad \text{(B2)}$$

where v and $f_{\rm LE}$ are calculated from

$$v(w,x) = \{2[w-U(x)]/m^*\}^{1/2} , \quad \text{(B3a)}$$

$$f_{\rm LE}(w,x) = \left[\frac{m^*}{2\pi kT_0}\right]^{1/2} n(x) e^{-[w-U(x)]/kT_0} . \quad \text{(B3b)}$$

The Boltzmann equation, now (B2), is thus a family of ordinary differential equations in the position variable with the total energy w simply a parameter.

The simplification embodied in Eq. (B2) has a physical justification as follows. The left-hand side of the Boltzmann equation expresses the change in f along the trajectories of the particles when collisions are neglected. Because the total energy w is conserved along a particle trajectory in the collisionless case, the total energy appears in (B2) only as an index to the trajectories, not as an independent variable. In these variables, we are integrating along the particle trajectories in space in a way similar to the well-known Chambers trajectory method[48] where one integrates along the trajectories in time. In actually calculating the distribution function, we find the deviation of f from $f_{\rm LE}$ rather than f itself in order to improve the accuracy of the calculation.

Solution of the Boltzmann equation. Our basic approach is to choose a mesh of total energies w and solve the Boltzmann equation (B2) sequentially for each of these energies. The spacing of the energy mesh is different depending on whether w is greater or less than the maximum of the potential energy, $U_{\rm max}$. For $w<U_{\rm max}$, the spacing of energies is uniform, while for $w>U_{\rm max}$, the energies are spaced so that the velocities $v=[2(w-U_{\rm max})/m^*]^{1/2}$ are uniformly spaced. Typically, we use a maximum energy of $U_{\rm max}+10kT_0$, 10 energy mesh points per kT_0 for $w<U_{\rm max}$, and 30 mesh points for $w>U_{\rm max}$. Thus we use, for example, 200–300 points for $T=300$ K and 800–900 points for $T=77$ K at $V_a=0.47$ V.

The first step in solving the Boltzmann equation is to decide what boundary conditions to apply to f at the edge of the structure ($x=-2.0$ μm and 2.4 μm). We have used long N^+ regions in order to damp out the effect of the boundaries and therefore use as the boundary condition at the edge of our N^+-N^--N^+ structure the analytic solution for f in a homogeneous field[7,23] given by E at the boundary. The boundary condition is applied to trajectories pointing towards the N^- region, $v>0$ at $x=-2.0$ μm and $v<0$ at $x=2.4$ μm; these trajectories are then followed until each crosses a boundary again either by crossing the entire structure ($w>U_{\rm max}$) or by reflecting from the potential barrier and recrossing the initial boundary ($w<U_{\rm max}$).

Having chosen the energy mesh and fixed the boundary conditions, we integrate the differential equation (B2) using a standard predictor-corrector or Runge-Kutta technique. In the case $w>U_{\rm max}$, the integration proceeds until the trajectory leaves the structure, while for $w<U_{\rm max}$ we integrate to a point close to the classical turning point. At the turning point, $v=0$ and (B2) cannot be integrated through this (integrable) singularity using standard methods. However, using a parabolic approximation to $U(x)$ near the turning point, it is straight forward to derive a connection formula between $f_+(w,x)$ and $f_-(w,x)$ in this region. Such a formula is used to reverse direction of integration at the turning point after which standard methods are again used to integrate along the trajectory until the boundary of the structure is reached. Repeating this procedure for each energy w yields the distribution function everywhere in the structure.

Obtain an output density. Once the distribution function is known by solving the Boltzmann equation, one must generate the density, $n_i^{\rm out}(x)$, which will be used to find the input density to the next iteration,

$$n_i^{\rm out}(x) = \int dv\, f(v,x) . \quad \text{(B4)}$$

In order to save storage space, the integral over f is performed as f is calculated. Since the input to each integration is simply the density and potential energy, the full distribution function on all approximately 150 000 meshpoints need never be stored.

Scale the density to maintain total charge neutrality. Having obtained the output density from the distribution function, we now force the total charge of the structure to be zero in order that the long-range electrostatic force of the ions and of the electrons balance. We accomplish this simply by multiplying $n_i^{\rm out}(x)$ by a constant a where

$$a = \int dx n_D(x) \Big/ \int dx\, n_i^{\rm out}(x) \quad \text{(B5)}$$

and the integrals extend over the entire N^+-N^--N^+ structure. The value of a is typically 1 ± 10^{-5}; hence, the effect of this scaling on the density profile is entirely negligible. The effect on the boundary electric field used in calculating the boundary value of f is, however, large—for $a=1\pm10^{-5}$, the excess charge creates a boundary field of about 3.6 kV/cm. This field is large compared to the boundary field calculated from the current carried ($\approx$40 V/cm), thus the charge-neutrality correction performed is essential.

Solve the screened Poisson equation. The next step in the iteration procedure is to use the density which has been corrected for charge neutrality to generate a new potential energy $U_i^{\rm out}(x)$. The simplest way to do this is, of course, to solve Poisson's equation which can be written in terms of the difference between the "in" and "out" density and potential energy as

$$\frac{d^2}{dx^2}(U_i^{\text{out}}-U_i^{\text{in}})=\frac{4\pi e^2}{\epsilon}(n_i^{\text{out}}-n_i^{\text{in}}) \ . \tag{B6}$$

We found that using (B6) led to oscillations of the charge density on successive iterations which severely impeded convergence; in particular, charge oscillated between the two N^+/N^- interfaces. In order to damp out these oscillations, we introduce some additional screening by adding the term

$$\frac{1}{\lambda^2}(U_i^{\text{out}}-U_i^{\text{in}}) \tag{B7}$$

to the right-hand side of Eq. (B6) where λ is a screening parameter. We solve the new equation using a simple Green function and $\lambda \approx L/2$ where L is the length of the N^- region in order to suppress oscillations between the two doping steps. Notice that near self-consistency when the difference between the out and in quantities is small, the additional screening has little effect on the result.

Mixing. The determination of $n_{i+1}^{\text{in}}(x)$ and $U_{i+1}^{\text{in}}(x)$ from the output quantities (a procedure known as mixing) is closely related to the way in which $U_i^{\text{out}}(x)$ is generated in order that the density and potential at self-consistency satisfy Poisson's equation. In fact, we use a mixing procedure such that n_i^{in} and U_i^{in} satisfy Poisson's equation for every i as follows:

$$U_{i+1}^{\text{in}}(x)=U_i^{\text{in}}(x)+b[U_i^{\text{out}}(x)-U_i^{\text{in}}(x)] \ , \tag{B8a}$$

$$n_{i+1}^{\text{in}}(x)=n_i^{\text{in}}(x)+b\left[n_i^{\text{out}}(x)-n_i^{\text{in}}(x)+\frac{\epsilon}{4\pi e^2\lambda^2}[U_i^{\text{out}}-U_i^{\text{in}}(x)]\right] \ , \tag{B8b}$$

where b is a small mixing parameter used to suppress oscillations. Usually we use different values of b for different iterations[49] in order to increase the average feedback per iteration $\langle b \rangle$. One successful choice is $b=0.35$ on every tenth iteration while $\beta=0.01$ otherwise ($\langle b \rangle=0.043$).

While this is the mixing scheme which we use, we cannot argue that it is the best, or even a very good, scheme to use. In fact, a mixing scheme which led to faster convergence would be very welcome since the number of iterations needed with our scheme is high because of the small value of $\langle b \rangle$. One possibility we have tried is to solve for U_i^{out} directly instead of the difference between U_i^{in} and U_i^{out} using a screened equation and then simply to mix back $U_i^{\text{out}}-U_i^{\text{in}}$ and $n_i^{\text{out}}-n_i^{\text{in}}$.[50] This method has performed well in surface electronic structure calculations.[50] We find for our problem that while the convergence rate is improved near self-consistency (by about a factor of 3), this method is much less stable for the initial iterations than the method presented above. We have not tried more sophisticated mixing procedures based either on more than one past iteration[51] or on Broyden's method.[52] Both of these types of procedures have proved useful in some electronic structure calculations[51,52] and may be worth pursuing in the present case.

Convergence. The iterative procedure presented above must be repeated many times before convergence is achieved. Typically, between 120 and 300 iterations are needed for the single-valley model depending on how effectively chosen are the two values of the mixing parameter. We look at three quantities to check the convergence: the change in density between input and output, the current as a function of distance, and the value of $f(v,x)$ at the edges of the structure.

The main test of convergence is to find the average change in density between input and output which for iteration number i is

$$\|\Delta n_i\|=\left[\sum_j [n_i^{\text{out}}(x_j)-n_i^{\text{in}}(x_j)]^2\right]^{1/2} \ . \tag{B9}$$

We typically iterate until $\|\Delta n_i\|<4\times10^{13}$ cm^{-3} from an initial value about 100 times larger. When this criterion is satisfied, $\Delta n_i(x)$ is largest in the N^- region but is everywhere less than 1×10^{14} cm^{-3} while the relative difference, $\Delta n_i/n_i^{\text{in}}$, is less than 1% everywhere.

The second test of convergence is to find the current from the distribution function at each point in space, $J(x)=-e\int dv v f(v,x)$. Because the Boltzmann equation that we use [Eq. (1) or (B2)] satisfies current continuity, $J(x)$ must be independent of x for the true solution. In fact, the current that we calculate varies slightly with distance, giving an indication of the degree of convergence. At $T_0=300$ K, the variation of $J(x)$ is about 1%, with most of the variation occurring near the doping steps. However, for the $T_0=77$ K results, the convergence of this quantity was substantially poorer for the same degree of convergence of the density: $J(x)$ varies by about 4% at $T_0=77$ K.

The third and final test of convergence is to look at the distribution function at the edge of the N^--N^--N^+ for velocities pointing away from the N^- ($v<0$ on the left-hand edge and $v>0$ on the right-hand edge). We apply a boundary condition to every trajectory pointing towards the N^- region from the edges but the values of $f(v,x)$ for trajectories pointing away from the N^- are unconstrained. We have assumed in applying the boundary condition that the N^+ region is long enough so that the distribution function at the edges of the structure is simply the homogeneous field distribution, $f_{\text{hom}}(v)$. We therefore test whether this is in fact the case for particles traveling away from the N^- region. The largest deviation of f from f_{hom}, which we will denote Δf, comes from the residual ballistic electron peak on the right-hand side of the structure where typically Δf is 10^{-4} times the maximum value of f. While this is a very small absolute error, the relative error is very large since f is small for this velocity ($f\approx10^{-7}$ of the maximum value of f). A more sensible way to evaluate Δf is to compare it to the difference between f_{hom} and the local equilibrium distribution, f_{LE} as this is the electric-field-induced change in the distribution. We find that Δf is about 1% of the maximum in $f_{\text{hom}}-f_{\text{LE}}$, i.e., the distribution is indeed nearly that for a uniform field so that we are justified in using f_{hom} for a boundary condition.

Two valleys: changes in the iterative procedure. Our treatment of the Γ valley follows closely the method for the single-valley case presented above. The use of the method of characteristics again results in a family of ordinary differential equations in x parametrized by the total

energy w. Formally, the equation for the Γ valley is similar to (B2). the main difference is the presence of two scattering rates on the right-hand side, one of which (the $\Gamma \rightarrow L$ rate) depends on v_Γ and hence on x through an equation similar to (B3a). Two small changes in method are necessary. (i) The boundary condition on f is that appropriate to the two-valley model, given in Ref. 23. (ii) When integrating the Boltzmann equation at constant w, one must treat with care the points at which the $\Gamma \rightarrow L$ rate turns on.

Our method of solution of the L-valley Boltzmann equation is substantially different from the single-valley method. We are forced to use an alternate method because the method used in the single-valley case requires a spatial mesh that is prohibitively fine. The spatial scale that enters the solution of the Boltzmann equation written in the variables w and x is a typical velocity times the scattering time, as can be seen from (B2). If we take a typical velocity in the L valley to be $v \approx (2kT_0/m_L^*)^{1/2} \approx 6\times 10^6$ cm/sec and use the intravalley scattering time $\tau_{LL} \approx 3\times 10^{-14}$ sec, we obtain $v\tau_{LL} \approx 0.002$ μm. The small value of this quantity compared to the corresponding value for the Γ valley (0.4 μm) indicates that a much finer spatial mesh is needed in the L valley because of the high effective mass and small scattering time.

However, the large effective mass and scattering rate also imply that the distribution is not strongly affected by either the applied field or the inhomogeneities; the short mean free path will suppress any nonequilibrium effects. We therefore assume that $f_L(v,x)$ can be parametrized by two quantities, the density $n_L(x)$ and the average velocity $\bar{v}_L(x)$, in the following way,

$$f_L(v,x) = n_L(x) \left[\frac{m_L^*}{2\pi k T_0} \right]^{1/2} \times \exp\left[-\frac{m_L^*[v-\bar{v}_L(x)]^2}{2kT_0} \right] . \tag{B10}$$

One can derive two coupled ordinary differential equations for $n_L(x)$ and $\bar{v}_L(x)$ from the Boltzmann equation, namely the current continuity equation and drift-diffusion equation. We rewrite these equations in terms of the variables $n_L(x)$ and $\eta(x) = n_L(x)\bar{v}_L(x)$,

$$\frac{d\eta}{dx} = -\frac{n_L - n_L^{\text{in}}}{\tau_{LL}} - \frac{n_L - n_{L,\text{joint}}^{\text{in}}}{\tau_{L\Gamma}} , \tag{B11a}$$

$$\frac{dn_L}{dx} = -\frac{eE}{kT_0} n_L - \eta \left[\frac{1}{\tau_{LL}} + \frac{1}{\tau_{L\Gamma}} \right] \frac{m_L^*}{kT_0} . \tag{B11b}$$

These equations can be readily solved using the same finite difference technique as that used for the coupled Poisson equation and drift-diffusion equation above [(Eq. (B1)].

Equations (B11) do not suffer from the same small length scale as the Boltzmann equation noted above because the distance over which $n_L(x)$ and $\eta(x)$ vary is the important scale. This scale is governed either by the variation in $E(x)$ which is the Debye screening length or by a typical velocity times the intervalley scattering time $\tau_{L\Gamma}$ which is much larger than the intravalley time τ_{LL}. Thus our mesh size is adequate for the solution of Eqs. (B11). Once we have reached self-consistency with this method, we do a few iterations using the Boltzmann equation for the L valley and a finer spatial mesh in order to check our results and calculate moments of the distribution. There is little difference between the Boltzmann equation results and the results of Eqs. (B11) for the voltages and temperature ($T_0 = 300$ K) considered in this work.

Once the output densities are found, the iterative procedure in the two-valley case is analogous to that for the single-valley case given above.

Two valleys: convergence. As in the single-valley case, the degree of convergence is tested by three quantities, the difference in output and input densities, the uniformity of the total current, and the deviation of $f_\Gamma(v,x)$ and $f_L(v,x)$ from the uniform-field result at the edge of the structure. In contrast to the single-valley case, the number of iterations needed is very large which suggests that other mixing schemes[51,52] should be investigated.

The degree of convergence of the density in the two-valley model is better than in the single-valley case throughout most of the structure; the norm of the deviation is $\|\Delta n_\Gamma\| \approx \|\Delta n_L\| \approx 2\times 10^{13}$ cm^{-3}. The region of greatest deviation is near the downstream N^+/N^- step where Δn_Γ and Δn_L are nearly of equal magnitude but opposite sign. Clearly the problem in this region is transfer between the Γ and L valleys which is not driven by a strong force (such as the electric field drives the total charge). In the region $x < 0.4$ μm there should be somewhat less transfer to the L valley while for $x > 0.4$ μm there should be more transfer to L. As for the single valley case the absolute differences correspond to relative differences of less than 1% for all x.

The uniformity of the current is much worse in the two-valley case than for a single valley, and it is because of this poor behavior that the two-valley model required so many iterations. The deviation of $J(x) = -e\int dv\, v[f_\Gamma(v,x)+f_L(v,x)]$ is largest near the downstream N^+/N^- step, again presumably due to $\Gamma \rightarrow L$ transfer. The total spread in $J(x)$ is about 4% for the two voltages 0.47 and 0.32 V, but is 6% for 0.82 V.

The final test of convergence is the deviation of the distribution function from the homogeneous field distribution, f_{hom}, for trajectories pointing away from the N^- region. The deviation for the Γ valley is about a factor of three smaller than for the single-valley above. For the L valley, the deviation relative to $f_{\max}$ is at the same level as in the single-valley case neglecting the ballistic peak, $\Delta f_L \approx 3\times 10^{-5} f_{L,\max}$. However because the drift velocity in the L valley is so small, the deviation of f_{hom} from $f_{L,\text{LE}}$ is small so that $\Delta f_L \approx 0.2(f_{\text{hom}} - f_{L,\text{LE}})_{\max}$. The small values for all three of these convergence criteria show that the calculation is indeed converged and that the N^+ region is long enough.

*Present address: AT&T Bell Laboratories 4G-314, Crawfords Corner Rd., Holmdel NJ 07733.

[1]A. B. Fowler, A. Harstein, and R. A. Webb, Phys. Rev. Lett. **48**, 196 (1982); W. J. Skocpol, L. D. Jackel, E. L. Hu, R. E. Howard, and L. A. Fetter, Phys. Rev. Lett. **49**, 951 (1982).

[2]K. S. Ralls, W. J. Skocpol, L. D. Jackel, R. E. Howard, L. A. Fetter, R. W. Epworth, and D. M. Tennant, Phys. Rev. Lett. **52**, 228 (1984); C. T. Rogers and R. A. Buhrman, *ibid.* **53**, 1272 (1984).

[3]T. W. Hickmott, P. M. Solomon, F. F. Fang, F. Stern, R. Fischer, and H. Morkoç, Phys. Rev. Lett. **52**, 2053 (1984); P. S. S. Guimares, D. C. Taylor, B. R. Snell, L. Eaves, K. E. Singer, G. Hill, M. A. Pate, G. A. Toombs, and F. W. Sheard, J. Phys. C **18**, L605 (1985).

[4]J. F. Ryan, R. A. Taylor, A. J. Turberfield, A. Maciel, J. M. Worlock, A. C. Gossard, and W. Wiegmann, Phys. Rev. Lett. **53**, 1841 (1984); Z. Y. Xu and C. L. Tang, Appl. Phys. Lett. **44**, 692 (1984); J. Shah, A. Pinczuk, A. C. Gossard, and W. Wiegmann, Phys. Rev. Lett. **54**, 2045 (1985).

[5]M. S. Shur and L. F. Eastman, IEEE Trans. Electron Devices **ED-26**, 1677 (1979).

[6]P. Hesto, J.-F. Pone, and R. Castagné, Appl. Phys. Lett. **40**, 405 (1982).

[7]H. U. Baranger and J. W. Wilkins, Phys. Rev. B **30**, 7349 (1984).

[8]P. Hesto, J.-F. Pone, R. Castagné, and J. L. Pelouard, in *The Physics of Submicron Structures,* edited by H. L. Grubin, K. Hess, G. J. Iafrate, and D. K. Ferry (Plenum, New York, 1984), p. 101.

[9]A. F. J. Levi, J. R. Hayes, P. M. Platzmann, and W. Wiegmann, Phys. Rev. Lett. **55**, 2071 (1985).

[10]M. Heiblum, M. I. Nathan, D. D. Thomas, and C. M. Knoedler, Phys. Rev. Lett. **55**, 2200 (1985).

[11]U. K. Reddy, J. Chen, C. K. Peng, and H. Morkoç, Appl. Phys. Lett. **48**, 1799 (1986).

[12]A. P. Long, P. H. Beton, and M. J. Kelly, Semicond. Sci. Technol. **1**, 63 (1986).

[13]For a review see H. L. Grubin, D. K. Ferry, G. J. Iafrate, and J. R. Barker, in *VLSI Electronics: Microstructure Science, Vol. 3,* edited by N. G. Einspruch (Academic, New York, 1982).

[14]S. M. Sze, *Physics of Semiconductor Devices,* 2nd ed. (Wiley, New York, 1981), p. 657.

[15]R. Stratton, Phys. Rev. **126**, 2002 (1962).

[16]C. Jacoboni and L. Reggiani, Rev. Mod. Phys. **55**, 645 (1985). For the case of small structures see, for example, P. Hesto, Surf. Sci. **132**, 623 (1983); Y. Awano, K. Tomizawa, and N. Hashizume, IEEE Trans. Electron Devices **ED-31**, 448 (1984); T. Wang and K. Hess, J. Appl. Phys. **57**, 5336 (1985).

[17]K. Blotekjaer, IEEE Trans. Electron Devices **ED-17**, 38 (1970); R. Bosch and H. N. Thim, *ibid.* **ED-21**, 16 (1974).

[18]H. L. Grubin and J. P. Kreskovsky, J. Vac. Sci. Technol. B **2**, 527 (1984).

[19]R. K. Cook and J. Frey, IEEE Trans. Electron Devices **ED-28**, 951 (1981).

[20]L. P. Kadanoff and G. Baym, *Quantum Statistical Mechanics* (Benjamin-Cummings, Menlo Park, California, 1962), pp. 102–110.

[21]C. Kittel, *Quantum Theory of Solids* (Wiley and Sons, New York, 1963), p. 308.

[22]The principal features of scattering by optic phonons in GaAs omitted by a relaxation time approximation are the discrete energy-loss structure, the strong forward scattering of the polar process, and the variation in energy of the intervalley process; see E. Conwell, in *Handbook on Semiconductors, Vol. 1,* edited by W. Paul (North-Holland, New York, 1982), p. 513.

[23]C. J. Stanton, H. U. Baranger, and J. W. Wilkins, Appl. Phys. Lett. **49**, 176 (1986).

[24]G. D. Mahan, J. Appl. Phys. **58**, 2242 (1985).

[25]S. A. Trugman and A. Taylor, Phys. Rev. B **33**, 5575 (1986).

[26]H. U. Baranger and J. W. Wilkins, Physica **134B**, 470 (1985). This preliminary report was based on results later found to be inadequately converged for some of the quantitative results, e.g., $x_E = 0.298$ μm not 0.305 as reported previously.

[27]J. J. Rosenburg, E. J. Yoffa, and M. I. Nathan, IEEE Trans. Electron Devices **ED-28**, 941 (1981).

[28]P. E. Schmidt, M. Octavio, and P. D. Esqueda, IEEE Electron Device Lett. **EDL-2**, 205 (1981).

[29]A. van der Ziel, M. S. Shur, K. Lee, T.-H. Chen, and K. Amberiadis, IEEE Trans. Electron Devices **ED-30**, 128 (1983).

[30]K. Tomizawa, Y. Awano, N. Hashizume, and M. Kawashima, IEE Proc. Pt. I **129**, 131 (1982).

[31]P. Hesto, Surf. Sci. **132**, 623 (1983).

[32]M. Hollis, N. Dandekar, L. F. Eastman, M. Shur, D. Woodard, R. Stall, and C. Wood, *Proceedings of the International Electron Devices Meeting, Washington, D.C., 1980* (IEEE, New York, 1980), p. 622; M. Hollis, L. F. Eastman, and C. E. C. Wood, Electron. Lett. **18**, 580 (1982).

[33]C. L. Allyn, A. C. Gossard, and W. Wiegmann, Appl. Phys. Lett. **36**, 373 (1980).

[34]H. Kroemer, Proc. IRE **70** (1982); D. Ankri and L. F. Eastman, Electron. Lett. **18**, 750 (1982).

[35]R. J. Malik, T. R. AuCoin, R. L. Ross, K. Board, C. E. C. Wood, and L. F. Eastman, Electron. Lett. **16**, 836 (1980).

[36]H. U. Baranger, Ph.D. thesis, Cornell University (University Microfilms International, Ann Arbor, 1986), pp. 35–37.

[37]K. Seeger, *Semiconductor Physics* (Springer-Verlag, New York, 1982), p. 234.

[38]D. E. Aspnes, Phys. Rev. B **14**, 5331 (1976).

[39]Within our single-valley approximation of the L valleys in GaAs, it is not appropriate to include the X valleys reported to be some 0.15 eV above the L valleys (D. E. Aspnes, Ref. 38).

[40]J. S. Blakemore, J. Appl. Phys. **53**, R123 (1982).

[41]Recently, C. J. Stanton has used an analytic solution for the two-valley model in bulk GaAs to calculate the noise spectrum (private communication). He finds that $\tau_{\Gamma L}^{-1}/\tau_{\Gamma\Gamma}^{-1} = 3.5$ fits both the noise data and the v-E data.

[42]The values of the relaxation rates used in the two-valley model discussed here are consistent with the scattering rates used in the more complex Monte Carlo calculations; see, for example M. A. Littlejohn, J. R. Hauser, and T. H. Glisson, J. Appl. Phys. **48**, 4587 (1977) or R. Castagné, Physica **134B**, 55 (1985).

[43]When one uses a larger mobility in the N^+ regions it is necessary to increase the length of the N^+ regions in order to apply uniform-field boundary conditions (Appendix B). We typically use 2μm-wide N^+ regions.

[44]Preliminary results of a Monte Carlo calculation with more realistic scattering rates indicates the presence of echo peaks in the energy distribution function [H. U. Baranger, J.-L. Pelouard, and R. Castagné (unpublished)].

[45]N. S. Wingreen, C. J. Stanton, and J. W. Wilkins, Phys. Rev. Lett. **57**, 1084 (1986).

[46]In a recent analytic calculation of the noise properties of the two-valley model, C. J. Stanton assumes that the $\Gamma \rightarrow L$ relaxation rate $\tau_{\Gamma L}$ mimics the $\Gamma \rightarrow L$ scattering rate in order to make the problem tractable (private communication).

[47]R. Courant and D. Hilbert, *Methods of Mathematical Physics*

(Interscience, New York, 1962), p. 28; M. D. Greenberg, *Foundations of Applied Mathematics* (Prentice-Hall, Englewood Cliffs, 1978), p. 569.

[48]R. Chambers, Proc. Phys. Soc., London, Sect. A **65**, 458 (1952); H. Budd, Phys. Rev. **127**, 4 (1962).

[49]P. H. Dederichs and R. Zeller, Phys. Rev. B **28**, 5462 (1983).

[50]R. M. Niemenen, J. Phys. F **7**, 375 (1977).

[51]H. Akai and P. H. Dederichs, J. Phys. C **18**, 2455 (1985).

[52]C. G. Broyden, Math. Comput. **19**, 577 (1965); J. E. Dennis, Jr. and J. J. Moré, SIAM (Soc. Ind. Appl. Math.) Rev. **19**, 46 (1977); P. Bendt and A. Zunger, Phys. Rev. B **26**, 3114 (1982); D. Vanderbilt and S. G. Louie, *ibid.* **30**, 6118 (1984).